Appl. Phys. B 70, 895–901 (2000) / Digital Object Identifier (DOI) 10.1007/s003400000260

Applied Physics B
Lasers
and Optics

Mobile laser spectrometer with novel resonant multipass photoacoustic cell for trace-gas sensing

M. Nägele, M.W. Sigrist

Swiss Federal Institute of Technology (ETH), Institute of Quantum Electronics, Laboratory for Laser Spectroscopy and Environmental Sensing, 8093 Zürich, Switzerland
(Fax: +41-1/633-1077, E-mail: sigrist@iqe.phys.ethz.ch)

Received: 23 November 1999/Published online: 19 April 2000 –

Abstract. The development and application of a mobile laser-photoacoustic spectrometer for in situ multicomponent monitoring of trace gases in different environments is reported. Sub-ppbV ($< 10^{-9}$ per volume)-concentrations can be measured with a novel resonant multipass photoacoustic cell. The cell is designed for flow mode operation in order to reduce adsorption effects. For ethene (C_2H_4) buffered in synthetic air a minimum detection limit of 70 ppt V (70×10^{-12} per volume) is achieved corresponding to a minimum measurable absorption coefficient $\alpha_{\min} = 2 \times 10^{-9}\,\mathrm{cm}^{-1}$ for a signal-to-noise ratio of 3. The multicomponent capability of the system is demonstrated with continuous sequential measurements of ethene, methanol, ethanol, CO_2, and H_2O of air from a fruit storage chamber.

PACS: 82.Ch

In comparison to more conventional gas detection schemes such as gas chromatography [1] photoacoustic (PA) spectroscopy [2] offers some distinct advantages such as the possibility of in situ measurements in flow mode operation (up to 2 litres/min) without any pre-concentration or pretreatment of the gas sample. Excellent detection sensitivity (down to sub-ppbV concentrations for intracavity arrangements) and a large dynamic range (up to 7 orders of magnitude) are achievable. The employed microphones represent simple room-temperature detectors that make costly detector cooling systems dispensable. The wavelength-independent responsivity of the PA detector implies that the same detector can be used for the whole wavelength range offered by the pump laser, i.e. for all gases absorbing in its spectral region.

Previous PA systems needed laser sources with minimum output powers on the order of tens of mW to W. By the implementation of a highly sensitive resonant multipass photoacoustic cell as described below, this disadvantage becomes less important because pump-laser sources at lower power levels can be employed. In combination with new low-power lasers the PA technique may open up additional application areas with all advantages of the PA technique. Other PA setups such as intracavity regimes also yield excellent detection limits [3, 4], however at the cost of a smaller dynamic range and higher sensitivity to beam pointing instabilities.

1 Experimental arrangement

1.1 General set-up

Figure 1 shows a schematic diagram of our current experimental set-up which represents a strongly modified version of an arrangement described in detail previously [5]. A line-tuneable sealed-off CO_2 laser (Ultra Lasertech, model 8122 V) with an active power stabilisation based on a piezo-driven out-coupling mirror is used as light source. An output power up to 6 W in the 10P and 10R branches and up to 4 W in the 9P and 9R branches is available on 74 different transitions. The diffraction grating is mounted in a Littrow arrangement. The grating angle is set to the desired laser transition with a computer-controlled step motor unit. After passing the chopper, the wavelength of the emission line can be checked by a spectrometer. Additionally a power meter records the laser power to normalise the photoacoustic (PA) signal S. The laser beam is coupled into the PA cell via a telescope. A novel resonant PA cell has been developed as described below. For the determination of the gas concentrations we measure the PA amplitude and phase, the cell pressure, the gas temperature, the CO_2 concentration, and the humidity. Depending on the application, the system offers the flexibility to measure further data such as the CO, NO, and CO_2 concentrations, recorded with an independent monitor (Maihak Multor 610) and different system temperatures as depicted in Fig. 1.

Possible gas temperature fluctuations occurring while operating the system in flow mode influence the speed of sound which results in a variation of the resonance frequency of the PA cell. The valid resonance frequency $f(T)$ at a given temperature T is determined from an initial resonance frequency measurement f_{T_0} at temperature T_0 by

$$f(T) = f_{T_0}(T/T_0)^{1/2}\,. \tag{1}$$

In order to reduce the influence of such fluctuations we implemented an active computer-controlled stabilisation of the

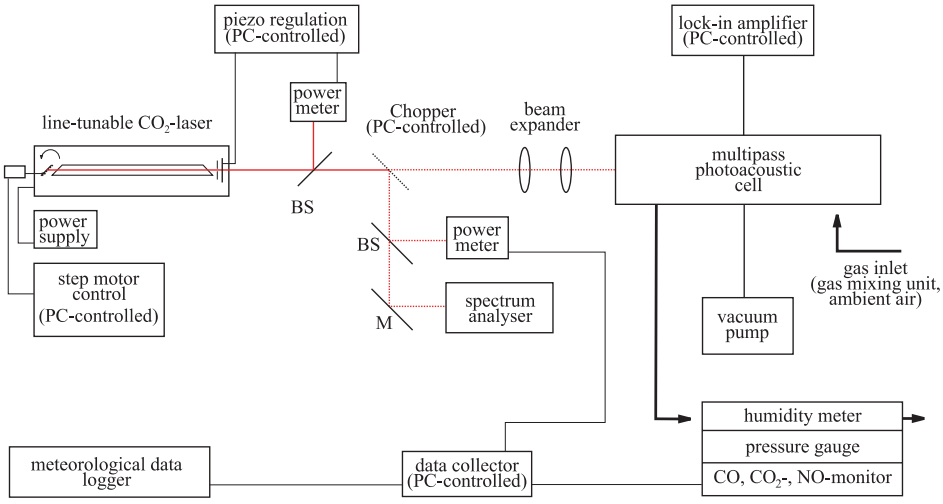

Fig. 1. Experimental set-up of the laser photoacoustic spectrometer (BS – beam splitter, M – mirror)

chopper frequency onto the cell resonance frequency. This is a crucial point for a completely automated operation of the system. The computer control of all system components ensures unattended continuous measurements over several days [5, 6]. The analysis of the measured PA amplitude and phase data to calculate the gas concentrations has been described in detail previously [6].

The whole CO_2-laser-based PA spectrometer is installed in a trailer and thus offers the possibility of field studies. For this purpose meteorological data (wind direction and velocity, and solar radiation) can be recorded in addition.

1.2 The multipass photoacoustic cell

We constructed a novel resonant multipass PA cell to record the PA signal, caused by the absorbed laser radiation, with a maximised signal-to-noise ratio (*SNR*). Figure 2 illustrates the set-up of the cell that basically consists of a Herriott-multipass arrangement [7] and a resonant PA cell [8–11].

In analogy to absorption spectroscopy, the PA signal and the *SNR*, depend on the available laser power. To obtain a preferably large PA signal at a given incident laser power P_0 we use a Herriott-multipass arrangement around the actual PA cell. With a mirror spacing of 70 cm, our Herriott cell exhibits 36 passes resulting in a total path length of 23.7 m. The number of passes can even be extended to 80 by a mirror adjustment. A He-Ne laser beam can be directed collinearly with the CO_2 laser beam over a flipper mirror for adjustment of the Herriott cell mirrors. The resonant PA cell which consists of cylinder, the actual resonator, and two adjacent buffer volumes with larger diameters, is placed inside the multipass arrangement. As a result more laser power P_{eff} is available inside the cell for the generation of the PA signal S than in a usual one-pass arrangement. Figure 3 shows the calculated power enhancement factor η versus the numbers of passes n in consideration of the transmission and reflection losses. The effective power P_{eff} is calculated as follows:

$$P_{\text{eff}} = P_0 \eta \,, \tag{2}$$

with

$$\eta = \sum_n T_{\text{trans}}^n \,. \tag{3}$$

The measured transmission coefficient per pass is $T_{\text{trans}} = 0.961$ (1 mirror and two windows). We are currently operating the cell with 36 passes because more passes render the

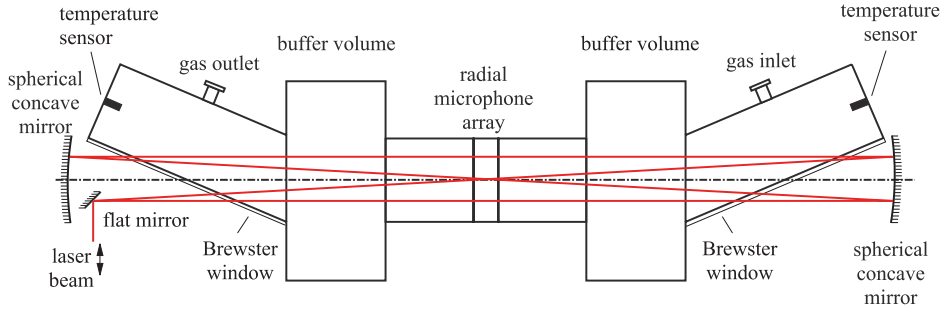

dimensions:

	length:	diameter:		
cell overall	700 mm	140 mm	number of microphones:	16
PA resonator	120 mm	50 mm	number of beam passes:	36
buffer volume	60 mm	120 mm	curvature radius of the mirrors:	1000 mm
optical path length	23680 mm			

Fig. 2. Multipass photoacoustic cell with Herriott cell, photoacoustic resonator, and cylindrical microphone array

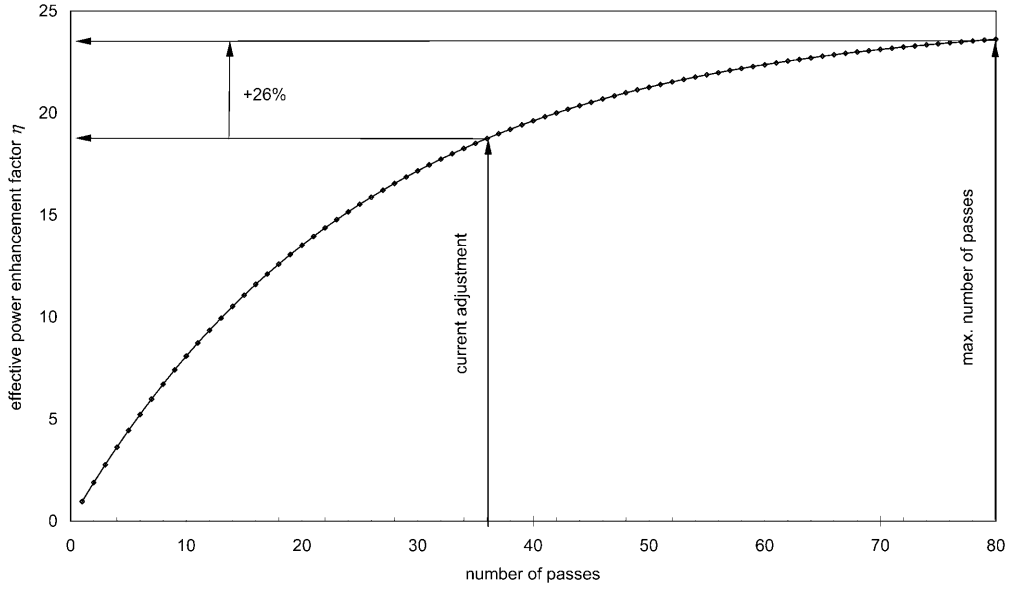

Fig. 3. Calculated effective power enhancement factor in dependence of the number of beam passes in the Herriott cell

adjustment of the cell more difficult and only yield an additional improvement η of 26%. The cell dimensions, particularly its diameter, are adapted to the number of passes and the beam diameter of the CO_2 laser. As Fig. 3 implies we achieve a power enhancement factor η of 19 with 36 passes.

The actual PA cell is sealed with Brewster windows on both ends. The inner cylindrical part enables the excitation of a pronounced longitudinal acoustic resonance whereas the buffer volumes with half of the resonator length reduce acoustic noise caused by the gas flow and by heating of the ZnSe-Brewster windows. The cell design was thus optimised to operate the cell on the first longitudinal resonance around 1250 Hz where the resonator length equals half the acoustic wavelength. At this resonance frequency we achieved the highest quality factor $Q \approx 70$ with this arrangement. In comparison to a non-resonant cell, the PA signal S_{res} is thus enlarged by the factor Q according to

$$S_{\mathrm{res}} = S_{\mathrm{nonres}}\, Q\ . \tag{4}$$

The measured frequency spectrum for our cell geometry is shown in Fig. 4. Apart from the first longitudinal resonance at 1250 Hz other less pronounced resonances appear at higher frequencies. They are due to higher longitudinal, radial, or azimuthal resonances but have not been assigned so far. The operation of the cell at the resonance frequency of 1250 Hz is advantageous, particularly in noisy environments, because the ambient noise is generally rather low at frequencies > 1 kHz. The rather large cell diameter required for the multipass arrangement limits the attainable quality factor. However, this is not a drawback for the system performance because the decreasing resonance width with increasing quality factor impedes the stabilisation of the chopper frequency on the resonance frequency. The signal fluctuation owing to the jitter of the chopper frequency results in a practical limit of $Q \approx 100$.

At the first longitudinal resonance the pressure amplitude reaches its maximum in the center of the resonator in a plane perpendicular to the optical axis. We implemented a radial microphone array with 16 electret microphones (Sennheiser

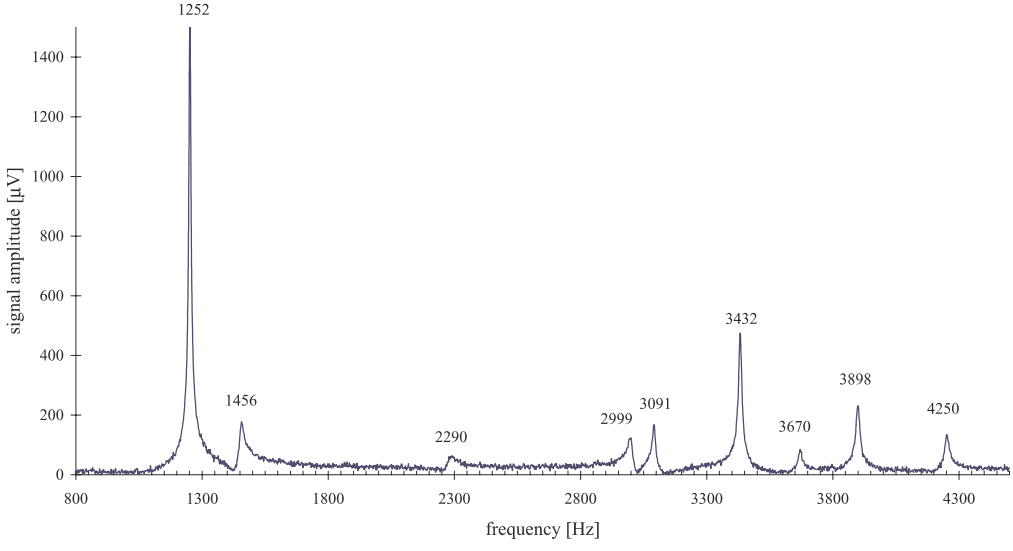

Fig. 4. Acoustic frequency spectrum of the multipass photoacoustic cell

KE 4-211-2) at this position of the resonator for the detection of the PA signal. The number m of microphones is limited by the dimension of the cell. The summation of the signals from the single microphones results in an m-times higher effective PA signal S_{tot}, i.e.

$$S_{\mathrm{tot}} = Sm \; . \tag{5}$$

On the other hand the (incoherent) noise only increases with $m^{1/2}$. One thus obtains

$$SNR_{\mathrm{tot}} = SNRm^{1/2} \; . \tag{6}$$

The final result of all three measures discussed above can be summarised as

$$S_{\mathrm{tot}} = G\eta QmS_{\mathrm{nonres}} \; . \tag{7}$$

The factor G is introduced to account for the off-axis propagation of the laser-beam passes through the cell. The expected increase of the microphone signal has experimentally been determined as $G = 3$. With $\eta = 19$, $Q = 70$, and $m = 16$ the total PA signal S_{tot} is enhanced by a factor of 64 000 compared to the signal amplitude S_{nonres} of a single-pass nonresonant cell operated at the same frequency. The signal enhancement also involves an increase of the background and the noise level. The *constant* background, for example caused by window heating and residual absorption by the mirrors, is subtracted from the signal as discussed below. The noise is composed of microphone noise (see (6)) and the noise originating from the jitter of the chopper frequency in connection to the resonance enhancement. The multipass arrangement increases the power by a factor of η (2). The power fluctuation of the laser thus also increases by the factor η. However, the multipass arrangement itself does not enhance the noise level any further but improves the detection limit considerably. A further aspect concerns the possibility to perform measurements at lower incident laser powers than would be feasible with single-pass cells.

The concentration c_{gas} of a single gas or a gas in a mixture under interference-free conditions, eventually diluted in a non-absorbing buffer gas, is now given by

$$c_{\mathrm{gas}} = \frac{S_{\mathrm{tot}}}{CN_{\mathrm{tot}}\sigma_{\mathrm{abs}}P_0} \; , \tag{8}$$

where N_{tot} denotes the total molecule density, σ_{abs} the absorption cross section of the gas at the selected laser transition, and C the cell constant. The cell constant is derived from (8) using a known gas concentration (in a certified gas mixture) and absorption cross section σ_{abs} resulting in a value of $C = 260\,\mathrm{V\,cm\,W^{-1}}$. The minimum detectable absorption coefficient α_{min} is given by

$$\alpha_{\mathrm{min}} = \frac{S_{\mathrm{tot,min}}}{CP_0} \; . \tag{9}$$

Under the assumption of a minimum measurable $S_{\mathrm{tot,min}}/P_0$ of $0.4\,\mu\mathrm{V\,W^{-1}}$ based on the (conservative) estimation of a detection limit that equals three times the standard deviation $\pm\sigma$, i.e. for $SNR = 3$, we obtain $\alpha_{\mathrm{min}} = 2 \times 10^{-9}\,\mathrm{cm^{-1}}$. This result is about an order of magnitude better than previous detection limits reported for extracavity PA gas monitoring [12].

The rather large cell volume of 2.3 l and the maximum gas flow of 1.5 l/min, which is limited by increasing ambient acoustic noise and onset of turbulence, yield a time resolution in flow mode of ≈ 5 min. This is still smaller than the time required to measure a complete spectrum with the line-tuneable CO_2 laser which takes 30 s per laser transition. The limiting factor for the minimum time resolution of the system is thus rather the tuning procedure in the case of multicomponent mixtures whereas it is the large cell volume for recording concentration fluctuations of single trace gases.

2 Measurements and results

2.1 Individual trace gases

In order to verify the expected excellent detection limits of our system, we measured ethene (C_2H_4) buffered in synthetic air (80% N_2, 20% O_2) at atmospheric pressure in flow mode at the 10P(14) laser transition where the absorption cross section σ_{abs} is maximum ($\sigma_{\mathrm{abs}} = 170 \times 10^{-20}\,\mathrm{cm^2}$ [6]). A computer-controlled gas mixing unit generates a cascade change of the concentration down to 0.15 ppbV. The result of this measurement is shown in Fig. 5. The inset implies a minimum detection limit of 0.07 ppbV after subtraction of the constant background signal caused by window heating. This background signal is shown in the last sequence of Fig. 5. It is recorded by measurements in a flow of synthetic air. The detection sensitivity achieved is comparable to data reported for intracavity arrangements [3, 4], however, without exhibiting their typical disadvantages such as sensitive signal behaviour related to the pointing stability of the laser beam or smaller dynamic range because the increasing intracavity absorption influences the laser performance.

In our former measurements [6, 13] performed with a single-pass resonant PA cell, 29 different gases were measured with $^{12}C^{16}O_2$ and $^{13}C^{16}O_2$ laser tubes. The corresponding minimum detection limits (for $SNR = 1$) for the different individual gases buffered in synthetic air, i.e. under interference-free conditions, are listed in the lower part of Table 1. In comparison to these former data the measurements on C_2H_4, CO_2, H_2O, methanol (CH_3OH), ethanol (C_2H_5OH), and benzene (C_6H_6) yielded 30 times lower detection limits (for $SNR = 3$) with our new cell. The present levels for ethene (70 pptV), methanol (0.2 ppbV), ethanol (0.5 ppbV), benzene (5 ppbV), CO_2 (770 ppbV), and H_2O (5 ppmV) are listed in italic in the upper part of Table 1. We expect that all previous detection limits in the lower part of Table 1 are now reduced by a factor of 30, or, when assuming $SNR = 1$ in both cases, by two orders of magnitude. However, this needs to be verified in further measurements.

2.2 Multicomponent gas monitoring in a fruit storage chamber

Besides low detection limits, multicomponent capability and a large dynamic range are important features of a gas sensor. The performance of our spectrometer regarding these two requirements has been evaluated with measurements on air samples from a fruit storage chamber, in collaboration with the Swiss Federal Research Station for Fruit-Growing,

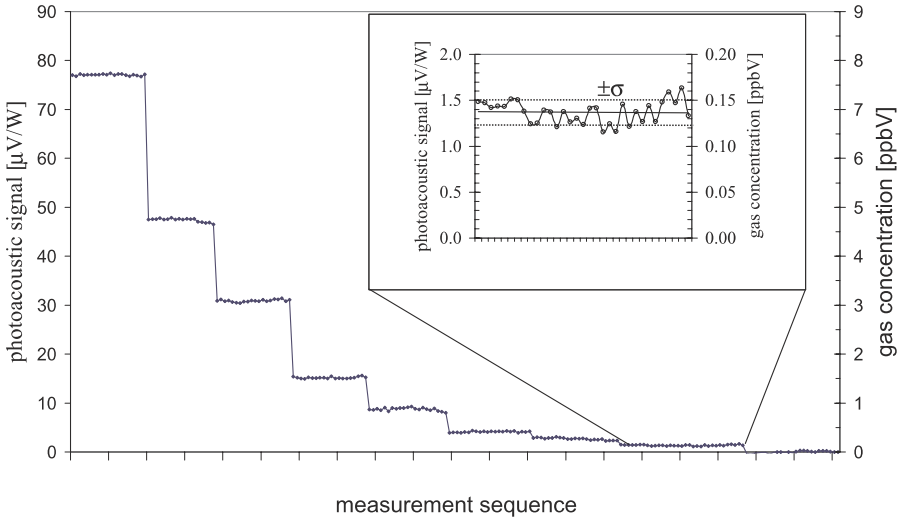

Fig. 5. Measurements of a cascade change of the ethene (C_2H_4) concentration buffered in synthetic air (80% N_2, 20% O_2) at room temperature and atmospheric pressure down to 0.15 ppb V, recorded at the 10P(14) laser transition. The *inset* shows an enlarged view of the measurements at 0.15 ppb V with the standard deviation $\pm\sigma$ as indicated

Table 1. Investigated compounds, maximum absorption cross section σ_{max} with corresponding $^{12}C^{16}O_2$ laser transition, and detection limits for interference-free conditions with $SNR = 1$ for the former data in the lower part of the table, and $SNR = 3$ (equivalent to the (conservative) estimation of a detection limit that equals three times the standard deviation $\pm\sigma$) for the data from this study in the upper part of the table

Substance	Formula	σ_{max}/ 10^{-20} cm^2	Laser line $^{12}C^{16}O_2$-isotope	λ/ cm^{-1}	c_{min}/ ppb V	Ref.
ethene	C_2H_4	170	10P(14)	949.48	0.07	a
methanol	CH_3OH	104	9P(34)	1033.48	0.2	a
ethanol	C_2H_5OH	31.8	9P(08)	1057.30	0.5	a
benzene	C_6H_6	11.1	9P(30)	1037.43	5	a
carbon dioxide	CO_2	0.023	9R(20)	1078.59	770	a
water	H_2O	0.0038	10R(20)	975.93	5000	a
ammonia	NH_3	319	9R(30)	1084.63	2	6
ozone	O_3	41.7	9P(14)	1052.19	13	6
1,3 butadiene	$C_4H_{10}O_2$	27.8	10P(46)	918.71	19	13
vinyl chloride	C_2H_3Cl	27.1	10P(22)	942.38	20	13
1,2 o-dichlorobenzene	$C_6H_4Cl_2$	21.1	9P(28)	1039.36	25	13
chlorobenzene	C_6H_5Cl	12.9	9R(30)	1084.63	41	13
m-dichlorobenzene	$C_6H_4Cl_2$	11.5	9R(20)	1078.59	46	13
propylene	C_3H_6	8.23	10P(36)	929.01	65	13
acrolein	C_3H_4O	7.71	10R(18)	974.62	69	13
γ-terpinen	$C_{10}H_{16}$	5.5	10P(36)	929.02	97	13
p-chlorobenzene	C_6H_5Cl	5.46	9R(34)	1086.86	98	13
toluene	C_7H_8	3.99	9P(36)	1031.47	134	6
isoprene	C_5H_8	3.1	10P(40)	929.97	172	6
ethyl benzene	C_8H_{10}	2.25	9P(36)	1031.47	237	13
o-xylene	C_8H_{10}	1.93	9P(12)	1053.92	277	13
isopentane	C_5H_{12}	1.72	10R(22)	977.21	310	6
acetone	C_3H_6O	1.26	10P(44)	920.83	424	13
p-xylene	C_8H_{10}	1.26	9P(38)	1029.44	424	13
m-xylene	C_8H_{10}	1.24	9P(24)	1043.16	430	13
$(\pm)$-α-pinene	$C_{10}H_{16}$	0.97	10P(08)	954.55	550	6
(1S)-(-)-β-pinene	$C_{10}H_{16}$	0.74	9P(12)	1050.44	721	6
ethyl bromide	C_2H_5Br	0.515	10P(20)	944.19	1040	13
methyl chloride	CH_3Cl	0.167	10P(44)	920.83	3200	13

a: This study

Viticulture and Horticulture (FAW) in Wädenswil/Zurich. Species of interest emitted by the fruits are ethene, methanol, ethanol, H_2O vapour, acetaldehyde, ethyl acetate, CO_2, and others [14–17]. Depending on storage conditions these gases represent key substances for fermentation processes and fruit quality in general. Within the frame of an extended FAW project on dynamically controlled atmospheres, the aim of our research was to record the concentrations of some of these gases as a function of time and to correlate the results with the ageing process of the fruits with the final goal to optimise the storage conditions.

We performed automated, unattended in situ measurements by placing our mobile trailer near a storage chamber containing Idared apples with a volume of 400 l. The chamber air was pumped continuously through our PA cell at a flow rate of 1 l/min without any pre-concentration or pre-treatment. The air was at atmospheric pressure and at a temperature of 4 °C. The pumping process, however, increased the air temperature to 20 °C in the PA cell. During the measurement the laser is tuned consecutively to different laser transitions. The determination of the concentration of each component of the mixture with our algo-

rithm [6] requires the measurement on at least one transition per compound. However, to improve the precision, we recorded the PA signal on two transitions for each compound, carefully selected for maximum absorption, minimum absorption interference, and good laser performance. In addition, we measured the PA signal on two laser transitions (10P(12), 10P(40)) for which all of the investigated gases exhibit negligible absorption to verify the constant background signal. Therefore, the spectra to monitor ethene (laser transitions: 10P(14), 10P(16)), ethanol (9P(08), 9P(32)), methanol (9P(34), 9P(36)), and CO_2 (10P(20), 9R(20)) comprise ten different laser transitions. For the analysis of our PA data we use measured calibration spectra of certified gas mixtures of the individual components buffered in synthetic air at atmospheric pressure. The absolute H_2O vapour concentration used for fitting our PA data is derived from the measured relative humidity and temperature. The high humidity (around 0.7% abs. corresponding to 95% relative humidity at 4 °C) and elevated CO_2 concentration (around 1%) posed a challenge to the mathematical analysis of the data. However, our Levenberg–Marquardt fitting algorithm [6] enabled us to determine reliable data for the four components with a precision of better than 20% even under these conditions. Unfortunately, the CO_2 concentrations of $\approx$ 1% present in the chamber air exceed the measurement range (1–1000 ppm V) of the NO/CO/CO_2 monitor so that our photoacoustically derived CO_2 data could not be compared with independent CO_2 data.

The daily measurements started after the chamber had been rinsed with pure nitrogen. In order to derive gas-emission rates per hour we recorded the temporal increase of the gas concentrations with a reduced time resolution of one spectrum/hour. Herewith we collected sufficient data for reliable results and saved needless laser operation time. Figure 6 presents the temporal development of the concentrations of the four components for a measurement period of three consecutive days. The apples were intentionally kept under anaerobic conditions with O_2 concentrations below 0.1% and CO_2 concentrations around 1%. In this case one expects a linear increase of the gas concentrations with time [18], i.e. constant emission rates. This behaviour is confirmed by our measurements. The emission rates obviously differ for the different compounds. The highest rates are observed for ethanol, the lowest for methanol. The exact rates, however, depend strongly on the previous storage conditions. Therefore, further comprehensive studies are needed to establish a firm correlation between the composition of the storage air and the fermentation and ageing processes of the apples. Our measurements demonstrated that the simultaneous monitoring of four of the relevant gas compounds mentioned above is feasible even under the given conditions of strong interferences.

3 Conclusions and outlook

The outstanding performance of our mobile automated laser spectrometer with respect to trace-gas monitoring has been demonstrated with measurements on individual trace gases and multicomponent gas mixtures. The implementation of a novel multipass resonant PA cell yields an improvement of the detection limits of two orders of magnitude for identical *SNR* compared to the previously used single-pass cell. Hence sub-ppbV concentration levels are now accessible with an extracavity arrangement which offers distinct advantages compared to intracavity set-ups such as the retention of the large dynamic range. In practice, a further reduction of minimum detectable concentrations is currently limited by fluctuations of system parameters, notably of the laser power and resonance frequency.

The possibility of in situ measurements in flow mode proves advantageous in several respects. The often important aspect, namely the falsification of derived trace-gas concentrations by adsorption of gas molecules on the walls of a sample bag or a measurement cell can thus be avoided or at least be drastically reduced.

The considerably improved detection limits open up new application areas for ultrasensitive gas sensing. On the other hand, tunable mid-IR lasers with lower power than the presently used CO_2 laser, such as diode-laser-based difference-frequency sources [19] or quantum cascade lasers [20, 21], can be employed. Thanks to their continuous tunability, these sources also reduce absorption interferences

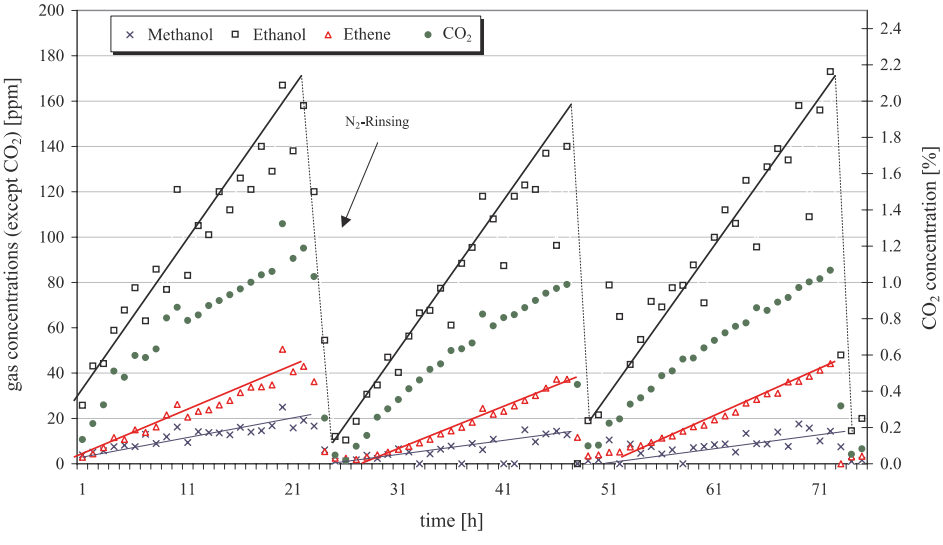

Fig. 6. Example of a three-day analytical study of air from a fruit storage chamber. The concentrations of four compounds are plotted versus time

in multicomponent mixtures that sometimes limit the detection selectivity achievable with the discretely tunable CO_2 laser.

Acknowledgements. This project is supported by the Swiss National Science Foundation, ETH Zurich, and the Alliance for Global Sustainability (AGS, AVINA funds). The measurements on the fruit storage chamber were done in collaboration with the Swiss Federal Research Station for Fruit-Growing, Viticulture and Horticulture in Wädenswil/Zurich.

References

1. G. Guiochon: Rev. Sci. Instrum. **61**, 3317 (1990)
2. M.W. Sigrist: In *Air Monitoring by Spectroscopic Techniques*, Vol. 127 ed. by M.W. Sigrist, Chemical Analysis Series (Wiley, New York 1994) Chapt. 4, pp. 163–238
3. T. Fink, S. Büscher, R. Gäbler, Q. Yu, A. Dax, W. Urban: Rev. Sci. Instrum. **67**, 4000 (1996)
4. F.J.M. Harren, F.G.C. Bijnen, J. Reuss, L.A.C.J. Voesenek, C.W.P.M. Blom: Appl. Phys. B **50**, 137 (1990)
5. A. Thöny, M.W. Sigrist: Infrared Phys. Technol. **36**, 585 (1995)
6. M. Moeckli, C. Hilbes, M.W. Sigrist: Appl. Phys. B **67**, 449 (1998)
7. J.B. McManus, P.L. Kebabian, M.S. Zahniser: Appl. Opt. **34**, 3336 (1995)
8. A. Karbach, P. Hess: J. Chem. Phys. **84**, 2945 (1986)
9. C. Hornberger, M. König, S.B. Rai, W. Demtröder: Chem. Phys. **190**, 171 (1995)
10. F.G.C. Bijnen, F.J.M. Harren, J. Reuss: Rev. Sci. Instrum. **67**, 2914 (1996)
11. P. Hess: Top. Curr. Chem. **111**, 1 (1983)
12. M.W. Sigrist: In *Encyclopedia of Spectroscopy and Spectrometry*, Vol. 3 ed. by J.C. Lindon, G.E. Tranter, J.L. Holmes (Academic Press, London 1999) pp. 1800–1809
13. P.L. Meyer, M.W. Sigrist: Rev. Sci. Instrum. **61**, 1779 (1990)
14. T.W. Kimmerer, T.T. Kozlowski: J. Plant Physiol. **69**, 840 (1982)
15. H.S.M. de Vries, F.J.M. Harren, L.A.C.J. Voesenek, C.W.P.M. Blom, E.J. Woltering, H.C.P.M. van der Valk, J. Reuss: J. Plant Physiol. **107**, 1371 (1995)
16. H.S.M. de Vries, M.A.J. Wasono, F.J.M. Harren, E.J. Woltering, H.C.P.M. van der Valk, J. Reuss: Postharvest Biol. Technol. **8**, 1 (1996)
17. F.B. Abeles, P.W. Morgan, M.E. Saltveit Jr.: *Ethylene in Plant Biology*, 1st edn. (Academic Press, San Diego 1992)
18. E.M. Yahia: Horticultural Rev. **16**, 197 (1995)
19. M. Seiter: PhD Thesis, No. 13354, Swiss Federal Institute of Technology (ETH) Zürich, Switzerland (1999) and series in Quantum Electronics Vol.14 (Hartung-Gorre, Konstanz)
20. J. Faist, F. Capasso, D.L. Sivco, C. Sirtori, A.L. Hutchinson, A.Y. Cho: Science **264**, 553 (1994)
21. F. Capasso, J. Faist, C. Sirtori, A.Y. Cho: Solid State Commun. **102**, 231 (1997)